MAX-PLANCK-INSTITUT FÜR PHYSIK

WERNER-HEISENBERG-INSTITUT

MPI-PhE/93-11
Mai 1993

Bose-Einstein Correlations in Neutrino and Antineutrino Interactions with Nucleons

Big Bubble Chamber Neutrino Collaboration

V.A. Korotkov[1], M. Aderholz[2], V.V. Ammosov[1], A.D. Andryakov[3], A.E. Asratyan[3], T. Coghen[4], O. Erriquez[5], G.S. Gapienko[1], V.A. Gapienko[1], J. Guy[6], G.T. Jones[7], V.S. Kaftanov[3], U.F. Katz[2], S.P. Krutchinin[3], M.A. Kubantsev[3], I.V. Makhlueva[3], P. Marage[8], D.R.O. Morrison[9], N. Schmitz[2], K.E. Varvell[7], W. Venus[6], W. Wittek[2], V.G. Zaetz[1]

[1]Institute of High Energy Physics, RU-142284 Protvino, Russia.
[2]Max-Planck-Institut für Physik, W–8000 München 40, Germany.
[3]Institute of Theoretical and Experimental Physics, RU-117259 Moscow, Russia.
[4]Institute of Nuclear Physics, PL-30055 Cracow, Poland.
[5]Dipartimento di Fisica dell'Università e Sezione INFN, I–70126 Bari, Italy.
[6]Rutherford Appleton Laboratory, Chilton, Didcot OX11 0QX, UK.
[7]University of Birmingham, Birmingham B15 2TT, UK.
[8]Inter-University Institute for High Energies, ULB–VUB, B–1050 Brussels, Belgium.
[9]CERN, CH–1211 Geneva 23, Switzerland.

8000 München 40 · Föhringer Ring 6

May 11, 1993

BOSE-EINSTEIN CORRELATIONS IN NEUTRINO AND ANTINEUTRINO INTERACTIONS WITH NUCLEONS

Big Bubble Chamber Neutrino Collaboration

V.A. Korotkov[1], M. Aderholz[2], V.V. Ammosov[1], A.D. Andryakov[3], A.E. Asratyan[3], T. Coghen[4], O. Erriquez[5], G.S. Gapienko[1], V.A. Gapienko[1], J. Guy[6], G.T. Jones[7], V.S. Kaftanov[3], U.F. Katz[2], S.P. Krutchinin[3], M.A. Kubantsev[3], I.V. Makhlueva[3], P. Marage[8], D.R.O. Morrison[9], N. Schmitz[2], K.E. Varvell[7], W. Venus[6], W. Wittek[2], V.G. Zaetz[1]

Abstract

Four data sets of charged current neutrino and antineutrino interactions with neon, deuterium and hydrogen collected from BEBC and the 15 Foot Bubble Chamber are used to study the Bose-Einstein correlations between like-sign charged pions. Two forms of the parametrization for the effect are used. No substantial differences are found between the data sets obtained with neon, deuterium and hydrogen targets. The Lorentz invariant parametrization of Goldhaber gives for the radius of the pion emission region the value $r_G = 0.80 \pm 0.04 \pm 0.16$ fm and for the chaoticity parameter the value $\lambda = 0.61 \pm 0.04 \pm 0.15$. Using the Kopylov-Podgoretskii parametrization yields $r_K = 1.27 \pm 0.06 \pm 0.12$ fm, $\lambda = 0.58 \pm 0.03 \pm 0.12$ and for the pion source lifetime $c\tau = 0.52 \pm 0.05 \pm 0.12$ fm. The Goldhaber parametrization was used to study the effect in further detail. The same emission radius and the same strength of the effect were found for particles produced in interactions on neutrons and protons. The data are compatible with a spherical shape of the pion emission region. No multiplicity or forward-backward dependences are found. No dependence of the effect on the event kinematical variables is seen.

[1]Institute of High Energy Physics, RU-142284 Protvino, Russia.
[2]Max-Planck-Institut für Physik, W–8000 München 40, Germany.
[3]Institute of Theoretical and Experimental Physics, RU-117259 Moscow, Russia.
[4]Institute of Nuclear Physics, PL-30055 Cracow, Poland.
[5]Dipartimento di Fisica dell'Università e Sezione INFN, I–70126 Bari, Italy.
[6]Rutherford Appleton Laboratory, Chilton, Didcot OX11 0QX, UK.
[7]University of Birmingham, Birmingham B15 2TT, UK.
[8]Inter-University Institute for High Energies, ULB–VUB, B–1050 Brussels, Belgium.
[9]CERN, CH–1211 Geneva 23, Switzerland.

1 Introduction

Bose-Einstein (BE) correlations are expected from basic quantum mechanical principles and originate from the symmetrization of the two-particle wave function of identical bosons. The details of the effect depend on the distribution of the source in space and time. The investigation of the BE effect is thus a powerful method for measuring the space-time dimension of the region from which identical bosons with similar momenta are emitted. The theory of this method was developed in the papers of Kopylov and Podgoretskii [1] and Cocconi [2]. An analogous method was first proposed by Hanbury-Brown and Twiss in astronomy to determine angular sizes of stellar objects [3].

In multiple hadron production the BE effect was first observed in a low energy $p\bar{p}$ annihilation experiment [4]. Subsequently, the sizes of pion emission regions have been determined in hadronic and nuclear interactions [5]-[18], in e^+e^- annihilation [19]-[27] and in lepton-nucleon interactions [28]-[30]. The radius of the pion emission region was found to be of the order of 1 fm in elementary particle collisions and several fm in nuclear collisions. Reviews of theoretical methods and experimental data concerning the BE interference effect have recently been given in [31]-[34].

One of the aims of this paper is to search for possible differences in the BE effect for pions produced in the interactions of (anti-)neutrinos on free and on bound nucleons. Such differences may exist, because after their generation inside nuclear matter pions can undergo rescattering before the stage of free propagation. It is commonly assumed that pair correlations of identical pions are determined by the relative positions of their last scattering points, which thereby play the role of sources. The BE effect can thus give information on the formation and propagation of hadrons in nuclear matter.

For the present analysis, four data sets of charged current neutrino and antineutrino interactions with neon, deuterium and hydrogen targets have been used, which were collected in the Big European Bubble Chamber (BEBC) at CERN and in the 15-Foot Bubble Chamber at Fermilab. A comparison of results from different data sets allows more reliable conclusions to be drawn.

In the next section various parametrizations for the BE interference effect are presented. Experimental details are given in section 3. The methods of analysis are explained in section 4. Results are presented and discussed in section 5 and conclusions are given in section 6.

2 The phenomenology of Bose-Einstein correlations

The strength of the BE correlation effect can be expressed in terms of the two-particle correlation function R, defined as

$$R(p_1, p_2) = D(p_1, p_2)/D_0(p_1, p_2), \tag{1}$$

where p_1, p_2 are the particle four-momenta, $D(p_1, p_2)$ is the measured two-particle density and $D_0(p_1, p_2)$ is the two-particle density in the absence of BE correlations.

Let us consider the simultaneous detection of identical pions (Fig. 1). We assume that the pions are emitted incoherently from two sources placed at points $\vec{r}_\alpha$ and $\vec{r}_\beta$, and are observed with momenta $\vec{p}_a$ and $\vec{p}_b$ at detectors a and b. According to quantum mechanics, the wave function describing the two pions must be symmetric under the exchange of the two pions:

$$\Psi = \frac{1}{\sqrt{2}}(\Psi_{a\alpha}\Psi_{b\beta} + \Psi_{b\alpha}\Psi_{a\beta}), \tag{2}$$

where $\Psi_{a\alpha}$ is the wave function for a pion produced at $\vec{r}_\alpha$ and observed at detector a, and so on. The correlation function then takes the form

$$R(p_a, p_b) = 1 + \cos(\vec{q} \cdot \vec{r}), \tag{3}$$

where $\vec{q} = \vec{p}_a - \vec{p}_b$, $\vec{r} = \vec{r}_\alpha - \vec{r}_\beta$. This expression shows that the BE effect measures the projection of the space distance between the sources on the direction of the momentum difference between the observed pions.

This picture of a two-point source can be generalized to a continuous distribution $\rho(\vec{x}, t)$ in space and time of sources emitting pions independently. The corresponding modified correlation function is

$$R(p_1, p_2) = 1 + |\tilde{\rho}(q)|^2, \tag{4}$$

where $q = p_1 - p_2$ and $\tilde{\rho}(q)$ is the Fourier transform of $\rho(\vec{x}, t)$.

A partial coherence of pion production reduces the correlation function $R(p_1, p_2)$. This reduction is usually accounted for by a chaoticity (or incoherence) parameter λ, first introduced in [5]:

$$R(p_1, p_2) = 1 + \lambda|\tilde{\rho}(q)|^2, \tag{5}$$

with $0 \leq \lambda \leq 1$. For totally incoherent sources, $\lambda = 1$ and $R = 2$ for $p_1 = p_2$. The BE effect thus allows one to probe the local space-time structure of the emitting source and is sensitive to its size, shape and coherence.

The full reconstruction of $\rho(\vec{x}, t)$ from $R(p_1, p_2)$ is difficult. Therefore the analysis of the experimental BE correlations is performed in terms of several parametrizations of the distribution $\rho(\vec{x}, t)$ or, equivalently, of the correlation function $R(p_1, p_2)$. Usually, two types of parametrizations are used:

- The Kopylov-Podgoretskii parametrization [1], which corresponds to a radiating spherical surface of radius r_K with incoherent point-like oscillators of lifetime τ:

$$R(q_t, q_0) = 1 + \lambda[4J_1^2(q_t r_K)/(q_t r_K)^2]/[1 + (q_0\tau)^2], \tag{6}$$

where J_1 is the first-order Bessel function, $\vec{p} = \vec{p}_1 + \vec{p}_2$, $q_0 = |E_1 - E_2|$, $q_t = |\vec{q} \times \vec{p}|/|\vec{p}|$. This parametrization is not Lorentz-invariant, and the variables are calculated in the centre of mass of the final-state hadrons.

- The Goldhaber parametrization [4, 35], which corresponds to a Gaussian shape of the source in the centre of mass of the pair, where $q_0 \equiv \Delta E = 0$:

$$R(\bar{M}^2) = 1 + \lambda \exp(-r_G^2 \bar{M}^2), \tag{7}$$

where $\bar{M}^2 = -(p_1 - p_2)^2 = M_{\pi\pi}^2 - 4m_\pi^2$, $M_{\pi\pi}$ being the invariant mass of the pion pair. This parametrization has the advantage of being rather simple and of having a Lorentz-invariant argument. It can also be written in terms of the Kopylov-Podgoretskii variables q_t and q_0 [31]:

$$R(q_t, q_0) = 1 + \lambda \exp[-r_G^2 q_t^2 - r_G^2 q_0^2/(\gamma^2 - 1)], \tag{8}$$

where γ is the γ-factor of the pion pair.

It has to be noted that the parameters r_K and r_G have different interpretations. At small q_t and q_0, however, the parametrization (6) can be approximated as

$$R(q_t, q_0) = 1 + \lambda \exp[-(r_K/2)^2 q_t^2 - (q_0\tau)^2]. \tag{9}$$

Comparing equations (8) and (9), the approximate relation $r_K \simeq 2r_G$ is expected.

3 Experimental data

The data used in the present analysis come from four bubble chamber experiments performed in the wide band neutrino and antineutrino beams of the CERN SPS and of the FNAL synchrotron at an incident proton energy of 400 GeV.

Two experiments, WA59 and E180, used a heavy neon-hydrogen mixture. The WA59 experiment employed the Big European Bubble Chamber BEBC at CERN, filled with 75 mole-% neon mixture (density 0.704 g/cm^3, radiation length 42 cm); muons were identified by a two-plane external muon identifier (EMI). The E180 experiment used the 15-Foot Bubble Chamber at Fermilab, filled with a 64 atomic-% neon mixture (density 0.74 g/cm^3, radiation length 39 cm); muons were identified by a one-plane EMI.

The WA21 and WA25 experiments were performed at CERN with BEBC, in beam conditions similar to those of the WA59 experiment. WA21 used a hydrogen

target, which permits one to investigate hadron production in clean conditions, as no nuclear effects distort the data. WA25 used a deuterium target, thus allowing one to study separately interactions on protons and on neutrons, and at the same time reducing to a minimum intranuclear reinteractions of produced particles.

The two experiments that use a heavy neon-hydrogen mixture (WA59 and E180), show very similar results, as expected. In the following, these data are combined and are called "Neon". The WA21 data are called "Hydrogen" and the WA25 data "Deuterium".

The (anti-)neutrino energy is determined in each event after correcting for the loss of neutral hadrons by a method based on transverse momentum balance. Further details on the four experiments can be found in [36]-[39].

For the following analysis, charged current events are selected with a muon momentum p_μ above 4 GeV/c. The total hadronic mass W is required to be above 2.5 GeV in order to select the kinematical region where multiple pion production is developed. The sizes of the final event samples are presented in Table 1.

All secondary charged particles were assumed to be pions, unless identified as a muon, an electron or a proton. The negative hadrons are mostly pions with a small kaon contamination. The positive hadrons include in addition a significant fraction of unidentified protons. Under these conditions the BE effect is expected to be more clearly seen for the negative hadrons.

The precision in the momentum and angle measurements is important for this investigation, because insufficient resolution tends to flatten the interference effect. For the analysis only hadrons with a fractional momentum measurement error $\Delta p/p$ below 30% are used. Corresponding losses are corrected for by a weighting procedure. The final results are however rather insensitive to this correction because the BE effect is determined by the ratio of the two-particle densities (see eq. (1)), such that the correction essentially cancels. The experimental resolution in $\bar{M}^2$ is estimated to be $\Delta\bar{M}^2 < 0.01$ GeV^2 at $\bar{M}^2 \approx 0.1$ GeV^2 for the Neon data; for Deuterium and Hydrogen it is better. The resolution improves strongly with decreasing $\bar{M}^2$. Such a resolution is entirely adequate to measure the radius of the pion emission region around an expected value of 1 fm.

In the subsequent analysis particle pairs with $\bar{M}^2 < 0.0002$ GeV^2 are not included. This both removes the few particles double-counted during measurement or reconstruction and also the main contribution from Dalitz pairs. It also excludes the region where Coulomb effects are significant (note that for the accepted data above $\bar{M}^2 = 0.0002$ GeV^2 the Coulomb effects are taken into account by the Gamow factors). There are only about 10 to 20 particle pairs excluded from each experiment. As a check, part of the analysis was repeated with $\bar{M}^2$ above 0.001 GeV^2. Since the results remained practically the same one may conclude that the residual contribution from Dalitz pairs is negligible.

Finally, only events with at least two hadrons of the same charge ($2h^-$ or $2h^+$)

are retained. The numbers of $(--)$, $(++)$ and $(+-)$ pairs available are given in Table 2.

4 The experimental method of studying the BE effect

4.1 Reference sample

The BE interference effect is usually studied by comparing the distributions for pairs of hadrons of like charge with those of unlike charge, at small values of the variables $\bar{M}^2$ or q_t. As an example Fig.2 presents the uncorrected $\bar{M}^2$ distributions of hadron pairs with negative $(--)$ and unlike $(+-)$ charge for the three data samples. The $(+-)$ distributions are normalized to the $(--)$ distributions in the interval $0.20 < \bar{M}^2 < 0.36$ GeV^2. The figure shows two differences between the distributions for $(--)$ and $(+-)$ pairs. Firstly, the $(--)$ exceeds the $(+-)$ distribution at small values of $\bar{M}^2$; this is a manifestation of the BE effect. Secondly, there is a small excess of the $(+-)$ over the $(--)$ distribution around $\bar{M}^2 = 0.5$ GeV^2 which is due to ρ meson production (see below).

The main experimental difficulty is to derive the reference two-particle density $D_0(p_1, p_2)$ in order to determine that part of the difference at small $\bar{M}^2$ that is to be attributed to the BE effect. Ideally, the reference sample for estimating $D_0(p_1, p_2)$ should be identical in all aspects to that of the like-charge pairs, except for the BE interference effect itself. Various methods for the construction of the reference sample have been proposed in the literature [31]-[34], in particular the following three:

A) The reference sample is formed of all $(+-)$ pairs, normalized to the number of $(--)$ pairs. In this method, however, resonances cause additional correlations.

B) The reference sample is formed adopting the so-called "mixed event" method: a hadron from one event is combined with a hadron of the same charge, randomly chosen from another event that has approximately the same characteristics. For this method, the events are subdivided into several bins of charged multiplicity (N_{ch}) and W. The momenta of the particles in one event are then rotated, such that the direction of the vector $\vec{q}_W = \vec{p}_\nu - \vec{p}_\mu$ coincides with that of the second event; pairs of hadrons are then formed. The number of pairs in the reference sample is normalised to the number of like-charge pairs in the same (N_{ch}, W) bin. This method is free from additional correlations due to resonances. However, correlations are lost, especially in the regions near the phase-space boundary, since in this method energy and momentum are not conserved.

C) The reference sample is formed by pairing unlike-charge hadrons from the same event, after the transverse momenta $\vec{p}_t$ of the hadrons (with respect to the current direction) have been randomly interchanged in the hadronic c.m.s. (The interchanging is carried out for the two components of p_t independently). The same normalization is used as for method A. This method is called the "reshuffled $\vec{p}_t$" method. It conserves the three-momentum, but energy conservation is slightly violated.

Another method for constructing the reference sample has been proposed [40] in a study of BE correlations in e^+e^- annihilation: correlations due to resonance decays and kinematical reflections are avoided by reflecting the momenta of all positive hadrons at a plane perpendicular to the sphericity axis.

4.2 Resonance contributions.

Correlations between identical pions produced in lepton-hadron interactions arise from several sources: conservation laws, dynamics, and BE statistics. The BE effect is the same for the $\pi^+\pi^+$ and $\pi^-\pi^-$ pairs, but dynamical effects (e.g. resonance production) and conservation laws can influence $\pi^+\pi^+$ and $\pi^-\pi^-$ systems in different ways. Such correlations are investigated using a simulation that does not contain the BE interference effect, namely the versions LEPTO 4.3 [41] and JETSET 6.3 [42] of the Lund Monte Carlo (MC) program. A value of 0.21 was chosen for the parameter $PAR(2) = P(s)/P(u)$, and all other parameters were set to their default values.

Figs. 3 and 4 show the MC predictions, as functions of $\bar{M}^2$ and q_t respectively, for various ratios of numbers of pion pairs. One observes that:

i) for pairs of pions that do not come from the same resonance, the ratios $(--)/(+-)$ and $(++)/(+-)$ are linear and approximately flat, decreasing only slightly at high $\bar{M}^2$ or q_t (curves 1 and 2);

ii) the contributions to $(++)$ and $(--)$ pairs from η' decays ($\eta' \to \eta\pi^+\pi^-, \eta \to \pi^+\pi^-\pi^0\,(\pi^+\pi^-\gamma)$) influence the region of small $\bar{M}^2$ or q_t at a level of 10 to 20% (curves 3 and 4);

iii) for νN interactions, there is a contribution from Δ^{++} decays, when the proton is misidentified as a pion (curve 5). For $\bar{\nu}N$ interactions (not shown), such a contribution is practically absent;

iv) the contributions to $(+-)$ pairs from η, η' and ω decays show rather strong variations at small $\bar{M}^2$. At higher $\bar{M}^2$, there is a large contribution from the ρ^0 resonance (Fig. 3b). For the distribution in q_t, the summed resonance contribution looks flatter (Fig. 4b).

However, the Lund model is not suitable for correctly estimating resonance production in neutrino interactions. It has been shown in several experiments [38, 39, 43, 44], that the average ρ^0 multiplicity in ν and $\bar{\nu}$ interactions is overestimated in the Lund model* by a factor 1.5 to 2. It is also known that $\eta\prime$ production is strongly overestimated in Lund fragmentation [10]. It should be stressed that the resonance contribution to $(+-)$ pairs can influence the BE study only if reference sample A is used, whereas the $\eta\prime$ contribution to $(--)$ and $(++)$ pairs directly modifies the apparent strength of the BE effect, whatever method is used.

4.3 Quality of the reference samples

For the present analysis, all three above mentioned methods of constructing the reference sample were tested, using a Monte Carlo (MC) program [45] that simulates (anti)neutrino events under the experimental conditions. Two variants of the program were used. The first contains a longitudinal phase space (LPS) model for simulating hadron production in neutrino-nucleon interactions, the second is based on the Lund fragmentation scheme. Neither variant contains BE correlations. The MC program includes the effects of hadron intranuclear rescattering, measurement errors and misidentification of charged hadrons. Samples of 100000 neutrino and 100000 antineutrino events were generated for each experiment, and the MC correlation functions, using methods A, B and C, were determined.

As an example, the MC correlation functions R^{--} and R^{++} are shown as functions of the variables $\bar{M}^2$ and q_t in Figs. 5 and 6 respectively, for the conditions of the WA59 experiment. Method C is seen to lead to a rather large artificial enhancement at low $\bar{M}^2$ and especially at low q_t. Therefore a modification of method C was tested (marked as C^* in the Figs. 5 and 6) in which the reshuffling of the transverse momentum components is done in the laboratory system. In this case, the artificial enhancement is somewhat smaller than before, but still sizable. The same conclusion was obtained by the NA22 collaboration [10]. On the other hand, the EMC collaboration [28] found that the correlation function obtained by method C with the Lund model is rather flat in the variable $\bar{M}^2$. They used a modification of method C in which the whole $\vec{p}_t$ was reshuffled between particles while in our approach the two components of $\vec{p}_t$ were reshuffled independently. Therefore the calculation of the correlation function was repeated exactly as in the EMC paper [28], but no significant differences were found as compared to the previous approach. It is therefore concluded that, at least for the present experimental conditions, method C is not well suited for deriving a reference sample, so that this method is not used in the following analysis.

The correlation function $R(\bar{M}^2)$ obtained by method B, using the Lund simula-

*This conclusion was obtained by comparing the data from these experiments with predictions of the Lund model version JETSET 5.2. But, as has been checked, the versions JETSET 5.2 and JETSET 6.3 give the same ρ^0 production rates for the conditions of these experiments.

tion, is reasonably flat, with only a small positive correlation at low $\bar{M}^2$; however, the LPS variant gives a significant peak at small $\bar{M}^2$. The behaviour of the correlation function in the variable q_t is even worse, since in addition to a peak at small q_t it shows a rather large slope with increasing q_t. Method B must therefore be used with caution.

Method A looks rather attractive for both variables. However, its obvious deficiency is the contribution of ρ^0 mesons to the $\pi^+\pi^-$ two-particle density, which reduces the correlation function $R(\bar{M}^2)$ in the range $0.36 < \bar{M}^2 < 0.64$ GeV^2 and, less strongly, the correlation function $R(q_t)$ in the range $0.6 < q_t < 0.8$ GeV/c. The use of method A therefore requires the removal of these kinematical regions from the analysis.

The above considerations on the quality of the reference samples lead us to apply methods A and possibly B when using the variable $\bar{M}^2$ and only method A when using the variable q_t.

The data were not corrected with the corresponding MC ratios as was done, for example, by the EMC collaboration [28], because the Lund model does not describe resonance production in neutrino reactions quantitatively.

4.4 Final-state interactions between pions

The final-state Coulomb interaction between produced pions distorts the two-particle densities of like and unlike charge pion pairs at small momentum differences. The attractive force between unlike-charge pions leads to an enhancement and the repulsive force between like-charge pions leads to a suppression. Usually this Coulomb effect is accounted for by introducing the Gamow factors [46] $G_{l(u)}(\eta)$ for like (unlike) charge pions

$$D^c_{l(u)}(p_1, p_2) = G_{l(u)}(\eta) D_{l(u)}(p_1, p_2), \tag{10}$$

where D^c and D are the two-particle densities in the presence and absence, respectively, of the Coulomb final-state interaction. The Gamow correction factors are given by:

$$\begin{aligned} G_l(\eta) &= \frac{2\pi\eta}{\exp(2\pi\eta) - 1}, \\ G_u(\eta) &= \frac{2\pi\eta}{1 - \exp(-2\pi\eta)}, \end{aligned} \tag{11}$$

with $\eta = \alpha m_\pi / \bar{M}, \alpha = 1/137$. This correction is rather small except for very small $\bar{M}^2$ values ($\simeq 3\%$ at $\bar{M}^2 = 0.01$ GeV^2), but is nevertheless taken into account because of its simplicity and for completeness. Technically, it was introduced into the data by weighting each like-charge pair by $1/G_l(\eta)$ and each unlike-charge pair by $1/G_u(\eta)$. The correction is twice as important for method A as for method B.

Final-state $\pi\pi$ rescattering generates a similar effect as the Coulomb interaction. This effect has been estimated [47], using experimentally determined phase shifts for $I = 0$ and $I = 2$ $\pi\pi$ scattering under the assumption that s-wave scattering is dominant at small momentum differences. The repulsive force in the $I = 2$ channel can reduce the measured correlation function by as much as 20%. The $I = 0$ channel may affect the correlation function if unlike-charge pairs are used for normalization (method A). However, the estimates of the $\pi\pi$ scattering effects have such large uncertainties that no attempt is made here to correct for them.

In experiments with nuclear targets, the correlation function may also be distorted by strong or Coulomb interactions between the emitted pions and the rest of the target nucleus. Experimentally, final-state Coulomb interaction between a pion and the rest of the nuclear system has been estimated using a crude approximation [15], and was found to be very small. All such distortions are ignored in the present analysis.

5 Results

In the following the ν and $\bar{\nu}$ data are combined for all experiments, unless special comments are made.

5.1 Fits with the Goldhaber parametrization

Figs. 7 and 8 show the correlation functions $R(\bar{M}^2)$ obtained by methods A and B, respectively. All plots show a BE enhancement at small values of $\bar{M}^2$. For $(--)$ pairs the enhancement is more significant and looks approximately the same for both methods used. For $(++)$ pairs the enhancement is smaller and the slope of the correlation function at high $\bar{M}^2$ depends on the method used.

The data points in Figs. 7 and 8 were fitted by the Goldhaber parametrization in the form:

$$R(\bar{M}^2) = \gamma[1 + \lambda \exp(-r_G^2 \bar{M}^2)](1 + \delta \bar{M}^2). \qquad (12)$$

The fit parameters are the normalization γ, the chaoticity λ, the spatial dimension of the pion source r_G and a linear slope δ of the background. The chaoticity parameter λ was introduced above as a measure of the incoherence of the pion emitters. On the other hand this parameter also accounts for the reduction of the BE signal by resonance production, particle misidentification and experimental resolution. The contribution of misidentified pions in like-charge pairs was studied by Monte Carlo. For negative hadrons about 90% of the pairs are true $\pi^-\pi^-$ pairs, practically independently of $\bar{M}^2$. For positive hadrons, the corresponding fraction is only $60-70\%$ at small $\bar{M}^2$ and slowly falls to $50-60\%$ at $\bar{M}^2 = 1$ GeV^2, with variations depending on the neutrino and target type. The parameter δ takes account of the variation of the correlation function at larger $\bar{M}^2$. It should be noted, however, that there

is no strong argument for the particular form $(1 + \delta\bar{M}^2)$ for this correction factor; therefore large variations of $R(\bar{M}^2)$ at large $\bar{M}^2$ can lead to some biases on the fitted parameters λ and r_G.

The fitted values of the parameters are presented in Tables 3 and 4 for $(--)$ and $(++)$ pairs respectively. The region $0.36 < \bar{M}^2 < 0.64$ GeV^2 was excluded from all fits when using method A, as discussed in section 4.3.

In Table 3 the fit results for Neon, Deuterium and Hydrogen are in good agreement when using method A. Furthermore, the Neon results obtained with method B are compatible with those obtained with method A, whereas the Hydrogen and Deuterium results for r_G and λ are 10 to 30% lower with method B than with method A. For all data sets the value of λ obtained with method B is 10 to 30% lower than with method A.

The results obtained for the Deuterium data with method A differ from those in [29]. The reason for this difference is that in [29] the ρ mass region was not excluded in the fits. Fitting the data of [29] excluding the ρ mass region yields a value for the radius which is very similar to the value of this paper.

For positive hadrons (Table 4), the situation is more complicated, the fitted values of λ and r_G obtained with method B being different from those obtained with method A for all data sets. The values of λ and r_G obtained with method A are more or less compatible for all three data sets.

A comparison of the parameters for $(++)$ and $(--)$ pairs shows that the chaoticity parameter λ is nearly 1.5 times as big for negative as for positive hadrons. This agrees with the relative proportions of true $\pi^-\pi^-$ pairs in the $(--)$ pairs and of true $\pi^+\pi^+$ pairs in the $(++)$ pairs given above. The same observation has been made in a number of experiments. For example, the NA22 collaboration found that the BE effect for identified positive pions was twice as strong as for all positive hadrons [10]. One also notices that the radius r_G is generally larger for $(++)$ pairs than for $(--)$ pairs, whatever method used.

To understand the difference in the values of λ and r_G for negative and positive hadron pairs, the BE effect, measured with method A, was simulated with the Lund Monte-Carlo for the conditions of the WA25 experiment. Like-charge pion pairs were assigned a weight according to (7), while other charged hadron pairs were assigned a weight of 1. As an illustration Figs. 9a and b show fitted values of chaoticity, λ_{fit}, and radius, r_{fit}, as functions of λ_{true}, i.e. the initial value used for the weight calculation according to (7). The initial value of the radius, r_G, was taken to be 0.8 fm. For negative pairs, a rather good agreement is observed between the input and output values for λ and r_G, down to $\lambda = 0.25$. In contrast, the positive pairs show large inconsistencies between the input and output values of λ and r_G. The tendency observed in Fig. 9 is that observed in the data: the fitted values of r_G are bigger for positive than for negative pairs and the λ_{fit} values are smaller for positive than for negative pairs. For both parameters the fit errors are larger for positive pairs.

As the $(--)$ pairs show a larger, cleaner and more stable signal, they are more suitable for a further investigation of the BE effect. Therefore only $(--)$ pairs are used in the following.

The difference in the values of λ and r_G for the three different data sets can not be considered as statistically significant for $(--)$ pairs. Therefore the correlation function $R^{--}(\bar{M}^2)$ was fitted in the form (12) to all three data sets simultaneously, the results being given in Table 3 as "All". One notices a reasonable quality of the fits, indicating that all data sets can be described by equation (12) with a single set of parameter values. (For $(++)$ pairs the same procedure yields only bad fits, see Table 4). Alternatively, the values of λ and r_G were constrained to be the same for all data sets, whereas different values of γ and δ were allowed for the different data sets. The fitted values of λ and r_G were the same as before, with $\chi^2/NDF = 55/52$ for method A and $\chi^2/NDF = 87/73$ for method B. If in addition different values of λ are allowed for different sets, the fit results for r_G are practically the same as before, namely $r_G = 0.80 \pm 0.04$ fm for method A and $r_G = 0.65 \pm 0.02$ for method B, while the values of λ are in the range 0.57 to 0.64 for method A and 0.44 to 0.50 for method B. One may thus conclude that the data sets are compatible and the best estimates of λ and r_G are obtained from the combined sample with method A. The differences between the results of methods A and B give conservative estimates of the systematical errors. The measured values of λ and r_G are then:

$$\begin{aligned} \lambda &= 0.61 \pm 0.04 \pm 0.15, \\ r_G &= 0.80 \pm 0.04 \pm 0.16 \text{ fm}. \end{aligned}$$

5.2 Fits with the Kopylov-Podgoretskii parametrization

The Kopylov-Podgoretskii parametrization (6) requires searching for the BE effect at small q_0 values. Therefore the data are divided into the following three q_0 intervals: $q_0 < 0.15$ GeV; $0.15 < q_0 < 0.40$ GeV, and $q_0 > 0.40$ GeV. The correlation function $R(q_t, q_0)$ for $(--)$ pairs obtained with method A is shown for the three q_0 intervals in Fig. 10. The number of $(+-)$ pairs is normalised to the number of $(--)$ pairs for the whole q_0 region. The data show an enhancement of $R(q_t, q_0)$ at small q_t for $q_0 < 0.15$ GeV and are rather flat for $q_0 > 0.40$ GeV. Table 5 gives the result of a simultaneous fit for the three q_0 intervals to the expression

$$R(q_t, q_0) = \gamma\{1 + \lambda[4J_1^2(q_t r_K)/(q_t r_K)^2]/[1 + (q_0\tau)^2]\}. \qquad (13)$$

The region $0.6 < q_t < 0.8$ GeV/c was excluded from the fit.

A similar procedure is adopted to study the dependence of the correlation function on q_0 in intervals of q_t. Three intervals are chosen: $q_t < 0.2$ GeV, $0.2 < q_t < 0.5$ GeV and $q_t > 0.5$ GeV. Again, in agreement with (6), an enhancement is observed (Fig. 11) at small q_0 only in the first two q_t intervals. The results of a simultaneous fit for the three q_t intervals are given in Table 6.

The fitted parameters for $R(q_t)$ and $R(q_0)$ are compatible within each data set which shows that the parameters are not affected by the binning of the two-dimensional function $R(q_t, q_0)$. The Deuterium and Hydrogen data give smaller values for the parameters r_K and τ than the Neon data, especially for the pion-source lifetime τ. Nevertheless, as in the previous section, all data sets were fitted simultaneously, the fit results being presented in Tables 5 and 6. A fit with different values of γ and λ for the different data sets changes the values of r_G and τ only slightly. Our best estimates of the parameters λ, r_K and τ are:

$$\begin{aligned} \lambda &= 0.58 \pm 0.03 \pm 0.12, \\ r_K &= 1.27 \pm 0.06 \pm 0.12 \text{ fm}, \\ c\tau &= 0.52 \pm 0.05 \pm 0.12 \text{ fm}, \end{aligned}$$

where the average differences between the results for the various data sets were taken as estimates of the sytematical errors. All values of the parameters agree quite well with those obtained by the TPC detector at PEP [19] in e^+e^- annihilation, namely $\lambda = 0.62 \pm 0.06 \pm 0.06$, $r_K = 1.27 \pm 0.07 \pm 0.08$ fm and $c\tau = 0.62 \pm 0.10 \pm 0.15$ fm.

Finally, comparing the values of the radius obtained with the Goldhaber (Table 3) and Kopylov-Podgoretskii (Tables 5 and 6) parametrizations it is seen that they do indeed fulfill the approximate relation $r_K \simeq 2r_G$, at a 20% level of accuracy.

5.3 Dependence on the incident neutrino type.

It is interesting to study the correlation function for neutrino and antineutrino interactions separately. From the curves 3 and 4 in Fig. 3a it is clear that one of the differences between ν and $\bar{\nu}$ interactions, expected on the basis of the Lund model without BE effect, is due to the different relative contributions of the $\eta\prime$ meson decay products to the like-charge pion pairs. Hence, the peak in the region of the BE effect for $(--)$ pairs should be slightly stronger in ν than in $\bar{\nu}$ interactions. The results of fitting the correlation function $R(\bar{M}^2)$ for $(--)$ pairs produced in ν and $\bar{\nu}$ interactions separately are given in Table 7. For each data sample, the fitted parameters for ν and $\bar{\nu}$ interactions are compatible at the level of 1σ to 1.5σ; however, the parameter λ is greater for ν than for $\bar{\nu}$ interactions in all cases. This result is in line, at least qualitatively, with the expected influence of the $\eta\prime$ resonance discussed above.

5.4 Dependence on the type of the target nucleon.

Neutrino and antineutrino scattering in deuterium allows one to study the BE correlations separately for interactions on protons and on neutrons. In principle, charged current neutrino (antineutrino) events with an even number of charged tracks (even prongs) should come from $\nu(\bar{\nu})n$ interactions and events with an odd number of

charged tracks (odd prongs) from $\nu(\bar{\nu})p$ interactions. However odd prong events can also be due to $\nu(\bar{\nu})n$ interactions where: i) the spectator proton gives a visible track in the chamber, or ii) hadrons produced in the primary interaction scatter from the spectator proton (rescattering).

The WA25 data were used to search for possible differences in the BE effect when (anti-)neutrinos interact with a proton or neutron. An event was classified as a $\nu(\bar{\nu})n$ interaction if it had either an even number of prongs, or an odd number including an identified proton in the backward direction. (Such a proton is a spectator proton, since in a $\nu(\bar{\nu})p$ interaction the secondary proton does not go backward in the laboratory system). All the remaining odd prong events were classified as $\nu(\bar{\nu})p$ interactions. The correlation functions $R^{--}(\bar{M}^2)$ for interactions on protons and neutrons were fitted to the form (12). The resulting fit parameters are given in Table 8. The values of λ and r_G for $\nu(\bar{\nu})p$ interactions are compatible with those from the Hydrogen sample in Table 3. There is no significant difference in the size of the pion emission region for interactions on protons and neutrons.

For completeness, the possible effects of rescattering and forward going spectator protons were estimated, using a weighting procedure as described in [49]. All events were classified into three groups: i) even-prong events (EP); ii) odd-prong events without visible spectator proton (OP); iii) events with a visible spectator proton (SP). Separate $\bar{M}^2$ distributions for neutron-target and proton-target events were obtained plotting each event first with a neutron-target weight W_n and then with a proton-target weight $W_p = 1 - W_n$, compensating for the effects of both rescattering and spectator-proton identification. The weight W_n was estimated as $W_n = W_{sp}/(1-f)$, where f is the fraction of events involving rescattering, while $W_{sp} = 0$ for OP events, $W_{sp} = 1$ for EP events and $W_{sp} = 1+[(E_s - P_s\cos\theta_s)/(E_s + P_s\cos\theta_s)]^2$ for SP events. Here E_s, P_s and θ_s are, respectively, the energy, the momentum and the production angle of the observed backward spectator proton. The value of the rescattering parameter f was taken to be $f = 0.12$ according to [50].

Table 8 shows that the correcting procedure practically does not change the fit parameters. One can thus conclude that no significant dependence of the BE effect on the type of the target nucleon is observed.

5.5 Shape of the pion emission region.

In section 2 it was shown that in the simplest case of two sources the correlation function depends on the scalar product of the difference vectors $\vec{q} = \vec{p}_1 - \vec{p}_2$ and $\vec{r} = \vec{x}_1 - \vec{x}_2$:

$$R = 1 + \cos(\vec{q}\cdot\vec{r}). \tag{14}$$

The BE effect thus measures the source size in the direction of the momentum difference $\vec{q}$, and gives the possibility of measuring the shape of the pion source.

To search for a possible non-spherical shape of the pion source, the data were divided for each experiment into two subsamples of hadron pairs, defined according

to the value of the angle θ between the momentum difference $\vec{q}$ and the virtual-boson momentum $\vec{q}_W$, calculated in the c.m.s. of the hadron pair. For pairs with $|\cos\theta| > 1/\sqrt{2}$, the BE effect measures the longitudinal dimension of the source (along the direction of $\vec{q}_W$), while for pairs with $|\cos\theta| < 1/\sqrt{2}$, it measures the transverse dimension of the source.

The results of fitting equation (12) to the correlation functions $R(\bar{M}^2)$ constructed from these subsamples are given in Table 9. The data are compatible with a spherical shape of the pion source as seen in the $\pi\pi$ rest frame.

5.6 Dependence on charged hadron multiplicity.

Hadronic experiments at high energies ($\sqrt{s} > 30$ GeV) have reported that the radius of the pion emission region increases with the charged hadron multiplicity N_{ch} (see e.g. [8]). At smaller energies no such multiplicity dependence was observed. The present data were divided into two subsamples for each experiment: a) events with $N_{ch} \leq 6$ and b) events with $N_{ch} > 6$. For each subsample, the radius of the pion emission region was measured using method A for the reference sample. The fit parameters are presented in Table 9. No sizeable difference in the fitted values of r_G is found between the different data sets.

If the multiplicity dependence of the source size is related to an increase of the particle density $\Delta n/\Delta y$ in rapidity (see e.g. [48]), this dependence of r_G on $\Delta n/\Delta y$ is probably too small to be observed in the present data.

5.7 Forward and backward pions.

In lepton-nucleon interactions the pions going forward in the hadronic c.m.s. come mainly from the fragmentation of the scattered quark, while pions going backward come from the spectator target remnant. The emission regions for pions going forward and backward can thus be different. The present data give, however, the same values of the source radius for backward and forward pions (see Table 9).

5.8 Dependence on the event kinematical variables.

In order to study the dependence of the BE parameters on the kinematical variables Q^2 (four-momentum transfer squared), W^2, $\nu = E_\nu - E_\mu$ and Bjorken-x, the data were divided into three regions for each variable, defined in such a way that each region contains approximately the same number of negative hadron pairs. The results of the BE analysis performed in each of these regions, using method A, are presented in Fig. 12a. No sharp dependence of r_G and λ on the kinematic variables is observed. Since all three data sets are in rather good agreement with each other, they were combined to search for possible dependencies, using a smaller binning in

the kinematic variables. The results are presented in Fig. 12b, leading to the same conclusion as above.

6 Summary and conclusions.

Bose-Einstein correlations were studied for negative and positive hadron pairs, using data of two $\nu(\bar{\nu})Ne$ experiments, a $\nu(\bar{\nu})D$ experiment and a $\nu(\bar{\nu})p$ experiment. Three methods were considered for the construction of the reference sample: unlike-charge pairs, mixed events and p_t reshuffling. The quality of these methods was checked using a Monte Carlo program that offered two possibilities for the hadron fragmentation: either the Lund model or an LPS model without resonance production. The p_t reshuffling method was rejected because of its behaviour at small $\bar{M}^2$ and q_t. Two parametrizations, the Goldhaber and the Kopylov-Podgoretskii form, were used to compare the data with theory.

The BE effect is seen in pairs of negative and in pairs of positive hadrons, the effect being stronger for negative hadrons. Such a behaviour is connected with the rather large contamination of the positive hadron sample by misidentified protons. A simple Monte Carlo simulation confirmed that the BE effect is weakened for positive hadrons. Therefore, only negative hadron pairs were used for further investigating the BE effect.

For the Goldhaber parametrization, the data sets yield the following best estimates for the chaoticity parameter and for the radius of the pion emission region:

$$\begin{aligned} \lambda &= 0.61 \pm 0.04 \pm 0.15, \\ r_G &= 0.80 \pm 0.04 \pm 0.16 \text{ fm}. \end{aligned}$$

These results are in agreement with those obtained in e^+e^- annihilation (e.g. [22]), μp interactions [28] and νA interactions [30].

For the Kopylov-Podgoretskii parametrization, the radius r_K turns out to be approximately twice as big as r_G, as expected. In this parametrization, the best estimates of the parameters are:

$$\begin{aligned} \lambda &= 0.58 \pm 0.03 \pm 0.12, \\ r_K &= 1.27 \pm 0.06 \pm 0.12 \text{ fm}, \\ c\tau &= 0.52 \pm 0.05 \pm 0.12 \text{ fm}. \end{aligned}$$

This is also in agreement with e^+e^- annihilation results [19].

The values of r_G do neither depend on the type of the neutrino nor on the type of the struck nucleon.

The shape of the pion emission region as viewed in the pion-pion rest frame is consistent with being spherical. The data do not show the dependence of the radius r_G on the charged hadron multiplicity that was observed in hadronic experiments

at high energies. No difference is found in λ and r_G for pions going forward and backward in the hadronic c.m.s.

No dependence of the values of r_G and λ on the kinematical variables Q^2, W^2, ν and Bjorken x was observed.

Acknowledgements. We express our gratitude to the CERN and Fermilab staff for the excellent beam conditions and bubble chamber operation. We gratefully acknowledge the careful work of the scanning and measuring staff in all the E180, WA21, WA25 and WA59 collaborating institutions. We are grateful to the WA21 and WA25 collaborations for kindly allowing us to use their data.

References

[1] G.I. Kopylov, M.I. Podgoretskii: Sov. J. Nucl. Phys. **15** (1972) 219; **18** (1973) 336; G.I. Kopylov: Phys. Lett. **B50** (1974) 472

[2] G. Cocconi: Phys. Lett. **B49** (1974) 459

[3] R. Hanbury Brown and R.Q. Twiss: Nature **178** (1956) 1046; **178** (1956) 1447

[4] G. Goldhaber et al.: Phys. Rev. Lett. **3** (1959) 181; Phys. Rev. **120** (1960) 300

[5] M.Deutschmann et al.: Nucl. Phys. **B204** (1982) 333

[6] V.V. Babintsev et al.: Sov. J. Nucl. Phys. **34** (1981) 412

[7] N. Akhababian et al.: Z. Phys. **C18** (1983) 97

[8] A. Breakstone et al.: Z. Phys. **C33** (1987) 333

[9] T. Åkesson et al. (AFS): Z. Phys. **C36** (1987) 517

[10] M. Adamus et al. (NA22): Z. Phys. **C37** (1988) 347

[11] J.L. Bailly et al. (NA23): Z. Phys. **C43** (1989) 341

[12] C. De Marzo et al.: Phys. Rev. **D29** (1984) 363

[13] U. Becker et al.: Nucl. Phys. **B151** (1979) 357

[14] D. Beavis et al.: Phys. Rev. **C27** (1983) 910

[15] W.A. Zajc et al.: Phys. Rev. **C29** (1984) 2173

[16] C. Albajar et al. (UA1): Phys. Lett. **B226** (1989) 410

[17] F. Rimondi (CDF): preprint FERMILAB-Conf-90/34-E (1990)

[18] M. Aguilar-Benitez et al. (NA27): Z. Phys. **C54** (1992) 21

[19] H. Aihara et al. (TPC): Phys. Rev. **D31** (1985) 996

[20] M. Althoff et al. (TASSO): Z. Phys. **C29** (1985) 347

[21] P. Avery et al. (CLEO): Phys. Rev. **D32** (1985) 2294

[22] I. Juricic et al. (MARK II): Phys. Rev. **D39** (1989) 1

[23] R. Walker et al. (AMI): KEK preprint 90-60, Ibaraki (1990), Submitted to the 25th Int. Conf. on High Energy Physics, Singapore, 1990

[24] O. Podobrin: Proc. 26th Recontre de Moriond, Les Arcs, France, p. 311 (1991)

[25] P.D. Acton et al. (OPAL): Phys. Lett. **B267** (1991) 143

[26] D. Decamp et al. (ALEPH): Z. Phys. **C54** (1992) 75

[27] P. Abreu at al. (DELPHI): Phys. Lett. **B286** (1992) 201

[28] M. Arneodo et al. (EMC): Z. Phys. **C32** (1986) 1

[29] D. Allasia et al. (WA25): Z. Phys. **C37** (1988) 527

[30] V.V. Ammosov et al. (SKAT): Sov. J. Nucl. Phys. **53** (1991) 609

[31] W. Hofmann: preprint LBL 23108 (1987)

[32] M.I. Podgoretskii: Physics of Elementary Particles and Atomic Nuclei, Vol.20, p. 628, Dubna (1989)

[33] B. Lörstad: Int. J. Mod. Phys. **A4** (1989) 2861

[34] D.H. Boal, C.-K. Gelbke, B.K. Jennings: Rev. Mod. Phys.**62** (1990) 553

[35] G. Goldhaber: LBL report, LBL-13291(1981) and Proc. Int. Conf. on High Energy Physics, Lisbon, Portugal, p. 767 (1981)

[36] V.V. Ammosov et al. (E180): Nucl. Phys. **B199** (1982) 399

[37] W. Wittek et al. (WA59): Z. Phys. **C40** (1988) 231

[38] D. Allasia et al. (WA25): Nucl. Phys. **B268** (1986) 1

[39] G.T. Jones et al. (WA21): Z. Phys. **C51** (1991) 11

[40] O. Podobrin: Proc. 20th Int. Symp. on Multiparticle Dynamics, Gut Holmecke, Germany, p. 417 (1990) (eds. R. Baier, D. Wegener, World Scientific, Singapore, 1991)

[41] G. Ingelman: The Lund Monte Carlo for Deep Inelastic Lepton-Nucleon Scattering, 1983

[42] T. Sjöstrand, M. Bengtsson: Comput. Phys. Commun. **43** (1987) 367

[43] V.V. Ammosov et al. (E180): Sov. J. Nucl. Phys. **45** (1987) 457

[44] W. Wittek et al. (WA59): Z. Phys. **C44** (1989) 175

[45] P. Kasper: A Monte Carlo Program for Neutrino and Antineutrino Interactions in Hydrogen, Deuterium and Neon-Hydrogen, Sept. 1985

[46] M. Gyulassy et al.: Phys. Rev. **C20** (1979) 2267

[47] R. Lednicky, V.L. Lyuboshits: Yad. Fiz. **35** (1982) 1316; M.G. Bowler: Z. Phys. **C39** (1988) 81; M. Suzuki: Phys. Rev. **D35** (1987) 3359

[48] A. Wroblewski: Proc. 25th Int. Conf. on High Energy Physics, Singapore, Vol. 1, p. 125 (1990) (eds. K.K. Phua, Y. Yamaguchi, World Scientific, Singapore, 1991)

[49] S. Barlag et al. (WA25): Z. Phys. **C11** (1982) 283; **C11** (1982) 281 (erratum); J. Hanlon et al., Phys. Rev. Lett. **45** (1980) 1817

[50] A.G. Tenner, NIKHEF-H/86-7 (1986)

Tables

Table 1: Number of CC events for various cuts

Selection	Beam	E180	WA59	WA25	WA21
$p_\mu > 4$ GeV/c	ν	5824	9837	22968	18711
	$\bar{\nu}$	6410	16938	15771	13128
$p_\mu > 4$ GeV/c	ν	4542	8011	18064	14180
$W > 2.5$ GeV	$\bar{\nu}$	4074	10983	10426	7916
$p_\mu > 4$ GeV/c	ν	3545	6362	15605	13569
$W > 2.5$ GeV	$\bar{\nu}$	2451	6978	7147	5060
≥ 1 like pair					

Table 2: Number of like and unlike charge hadron pairs used in the analysis ($P_\mu > 4$ GeV/c, $W > 2.5$ GeV)

Exp.	Beam	$(--)$	$(++)$	$(+-)$
Neon	ν	11476	36560	55603
	$\bar{\nu}$	17602	17665	48775
Deuterium	ν	19251	57758	98381
	$\bar{\nu}$	15690	10359	39382
Hydrogen	ν	11854	60375	79220
	$\bar{\nu}$	9996	9761	30990

Table 3: Results of fitting equation (12) to the correlation function $R(\bar{M}^2)$ for $(--)$ pairs in Figs. 7a and 8a, obtained with method A and B respectively

	Exp.	γ	λ	r_G, fm	δ, GeV^{-2}	χ^2/NDF
A	Neon	0.97±0.02	0.65±0.07	0.81±0.07	-0.06±0.03	11.8/16
	Deuterium	0.95±0.02	0.56±0.05	0.73±0.07	-0.01±0.03	20.0/16
	Hydrogen	1.01±0.02	0.67±0.08	0.86±0.08	-0.11±0.03	20.9/16
	All	0.98±0.01	0.61±0.04	0.80±0.04	-0.06±0.02	66.9/56
B	Neon	0.99±0.02	0.56±0.06	0.80±0.07	-0.13±0.02	21.2/23
	Deuterium	0.90±0.04	0.48±0.06	0.49±0.05	-0.04±0.04	31.1/23
	Hydrogen	0.97±0.03	0.44±0.06	0.63±0.08	-0.12±0.03	23.9/23
	All	0.97±0.02	0.46±0.03	0.64±0.04	-0.11±0.02	87.2/77

Table 4: Results of fitting equation (12) to the correlation function $R(\bar{M}^2)$ for $(++)$ pairs in Figs. 7b and 8b, obtained with method A and B respectively

	Exp.	γ	λ	r_G, fm	δ,GeV^{-2}	χ^2/NDF
A	Neon	0.90±0.01	0.51±0.10	1.35±0.17	0.26±0.02	16.5/16
	Deuterium	0.90±0.01	0.47±0.06	1.06±0.10	0.26±0.02	27.6/16
	Hydrogen	0.90±0.01	0.45±0.10	1.40±0.19	0.28±0.02	17.8/16
	All	0.90±0.01	0.46±0.05	1.23±0.08	0.27±0.01	80.6/56
B	Neon	0.91±0.05	0.34±0.06	0.44±0.06	0.01±0.05	45.0/23
	Deuterium	0.98±0.02	0.37±0.03	0.60±0.05	-0.09±0.02	31.8/23
	Hydrogen	1.03±0.01	0.25±0.05	0.97±0.14	-0.11±0.01	49.8/23
	All	0.97±0.02	0.28±0.02	0.54±0.06	-0.06±0.02	167/77

Table 5: Results of fitting equation (13) to the correlation function $R(q_t)$ for $(--)$ pairs in Fig. 10, for the three q_0 intervals

Exp.	γ	λ	r_K, fm	$c\tau$, fm	χ^2/NDF
Neon	0.90±0.01	0.71±0.07	1.44±0.10	0.74±0.11	50.5/44
Deuterium	0.89±0.01	0.46±0.04	1.19±0.09	0.39±0.07	62.8/44
Hydrogen	0.85±0.02	0.69±0.06	1.18±0.10	0.51±0.09	46.4/44
All	0.89±0.01	0.58±0.03	1.27±0.06	0.52±0.05	182.0/140

Table 6: Results of fitting equation (13) to the correlation function $R(q_0)$ for $(--)$ pairs in Fig. 11, for the three q_t intervals

Exp.	γ	λ	r_K, fm	$c\tau$, fm	χ^2/NDF
Neon	0.89±0.01	0.66±0.06	1.22±0.06	0.63±0.10	43.4/44
Deuterium	0.88±0.01	0.52±0.04	1.12±0.05	0.35±0.06	52.8/44
Hydrogen	0.87±0.01	0.72±0.07	1.13±0.06	0.54±0.08	51.9/44
All	0.88±0.01	0.60±0.03	1.15±0.03	0.47±0.04	163.8/140

Table 7: Results of fitting equation (12) to the correlation function $R(\bar{M}^2)$ for $(--)$ pairs in neutrino and antineutrino interactions, obtained by method A

Target	Beam	γ	λ	r_G, fm	δ, GeV^{-2}	χ^2/NDF
Neon	ν	0.95±0.03	0.77±0.11	0.83±0.09	-0.02±0.04	10.0/16
	$\bar{\nu}$	0.98±0.03	0.55±0.08	0.78±0.10	-0.07±0.04	15.3/16
Deuterium	ν	0.97±0.03	0.63±0.07	0.76±0.08	-0.05±0.03	16.2/16
	$\bar{\nu}$	0.91±0.05	0.49±0.08	0.67±0.11	0.11±0.06	22.0/16
Hydrogen	ν	1.00±0.03	0.83±0.10	0.83±0.08	-0.12±0.03	18.3/16
	$\bar{\nu}$	0.98±0.03	0.46±0.11	0.88±0.17	-0.04±0.05	20.4/16

Table 8: Results of fitting equation (12) to the correlation function $R(\bar{M}^2)$ for $(--)$ pairs from the WA25 experiment, obtained with method A. Results are given uncorrected and corrected for rescattering and forward proton spectators, separately for interactions on protons and neutrons

Target	γ	λ	r_G, fm	δ, GeV^{-2}	χ^2/NDF
			Uncorrected		
p	0.97±0.03	0.54±0.07	0.78±0.09	-0.03±0.03	16.9/16
n	0.91±0.05	0.60±0.09	0.67±0.09	0.04±0.06	21.6/16
			Corrected		
p	0.98±0.03	0.54±0.08	0.79±0.10	-0.03±0.04	16.7/16
n	0.91±0.05	0.60±0.09	0.67±0.09	0.04±0.06	21.7/16

Table 9: Results of fitting equation (12) to the correlation function $R(\bar{M}^2)$ for $(--)$ pairs, obtained with method A, for different regions of the angle θ and the charged multiplicity N_{ch}, and for forward and backward hadrons

	Neon		Deuterium		Hydrogen	
	λ	r_G, fm	λ	r_G, fm	λ	r_G, fm
$\lvert\cos\theta\rvert > 1/\sqrt{2}$	0.68±0.08	0.81±0.08	0.63±0.07	0.78±0.07	0.76±0.10	0.89±0.09
$\lvert\cos\theta\rvert < 1/\sqrt{2}$	0.55±0.12	0.82±0.15	0.41±0.12	0.53±0.12	0.42±0.11	0.72±0.19
$N_{ch} \leq 6$	0.51±0.08	0.76±0.11	0.46±0.07	0.64±0.10	0.56±0.12	0.91±0.14
$N_{ch} > 6$	0.77±0.10	0.83±0.09	0.62±0.08	0.78±0.09	0.68±0.10	0.85±0.10
Forward	0.75±0.10	0.73±0.09	0.61±0.09	0.60±0.08	0.67±0.11	0.93±0.12
Backward	0.63±0.11	0.91±0.13	0.61±0.11	0.68±0.13	1.07±0.19	0.83±0.12

Figure captions

Fig. 1 : Schematic illustration of the Bose-Einstein effect.

Fig. 2 : $\bar{M}^2$ distributions for $(--)$ (dots) and $(+-)$ (histogram) pairs for the three data samples (neutrino and antineutrino combined). The $(+-)$ distributions are normalized to the $(--)$ distributions in the region of $0.20 < \bar{M}^2 < 0.36$ GeV^2 .

Fig. 3 : (a) predictions of the Lund Monte-Carlo for the ratios of the following numbers, as functions of $\bar{M}^2$: 1) $\pi^+\pi^+(\pi^-\pi^-)$ pairs to $\pi^+\pi^-$ pairs in $\nu(\bar{\nu})N$ interactions, where the two pions of a pair do not come from the same resonance; 2) $\pi^-\pi^-(\pi^+\pi^+)$ pairs to $\pi^+\pi^-$ pairs in $\nu(\bar{\nu})N$ interactions, where the two pions of a pair do not come from the same resonance; 3) $\pi^-\pi^-(\pi^+\pi^+)$ pairs from $\eta\prime$ decays to all $\pi^-\pi^-(\pi^+\pi^+)$ pairs in $\nu(\bar{\nu})N$ interactions; 4) $\pi^+\pi^+(\pi^-\pi^-)$ pairs from $\eta\prime$ decays to all $\pi^+\pi^+(\pi^-\pi^-)$ pairs in $\nu(\bar{\nu})N$ interactions; 5) $\pi^+\pi^+$ pairs from Δ^{++} decay to all $\pi^+\pi^+$ pairs in νN interactions (protons with momentum greater than 1 GeV/c were taken as pions); (b) predictions of the Lund Monte-Carlo for the relative resonance contributions to the $\bar{M}^2$ distribution, defined as a ratio of the number of $\pi^+\pi^-$ pairs from a particular resonance decay ($\rho^0, \omega, \eta\prime, \eta$) to all $\pi^+\pi^-$ pairs in νN interactions.

Fig. 4 : The same as for Fig.3, for the variable q_t.

Fig. 5 : Correlation function $R(\bar{M}^2)$ (a) for pairs of negative hadrons; (b) for pairs of positive hadrons, from a Monte Carlo simulation under the conditions of the WA59 experiment. Different methods (marked as A, B, C and C*) were used for the construction of the reference sample and two variants for the hadron fragmentation in neutrino-nucleon scattering were tested, namely the Lund model (open circles) and an LPS model (crosses).

Fig. 6 : The same as for Fig.5, but for the correlation functions $R(q_t)$.

Fig. 7 : Correlation functions $R(\bar{M}^2)$ (a) for pairs of negative hadrons; (b) for pairs of positive hadrons, obtained with method A. The solid curves show the fits of parametrization (12) to each data set separately; the dashed curves show the simultaneous fit to all data sets.

Fig. 8 : The same as for Fig.7, but using method B.

Fig. 9 : Fitted values of (a) λ_{fit} and (b) r_{fit} for pairs of positive and pairs of negative hadrons as a function of λ_{true}, obtained by method A from a Monte Carlo simulation of the BE effect under the conditions of the WA25 experiment. The input value of the radius r_G was taken to be 0.8 fm.

Fig. 10: Correlation functions $R(q_t, q_0)$ for pairs of negative hadrons, obtained with method A, as a function of q_t for three q_0 regions: a) $q_0 < 0.15$ GeV; b) $0.15 < q_0 < 0.40$ GeV; c) $q_0 > 0.40$ GeV. The solid curves show the fits of parametrization (13) to each data set separately; the dashed curves correspond to the simultaneous fit of all data sets.

Fig. 11: Correlation functions $R(q_t, q_0)$ for pairs of negative hadrons, obtained with method A, as a function of q_t for three q_0 regions: a) $q_t < 0.2$ GeV; b) $0.2 < q_t < 0.5$ GeV; c) $q_t > 0.5$ GeV. The solid curves show the fits with parametrization (13) to each data set separately; the dashed curves show the simultaneous fit to all data sets.

Fig. 12: Chaoticity parameter λ and radius r_G of the pion emission region as functions of the kinematical variables Q^2, W^2, ν and x_B from fitting eq. (12) (a) to the Neon (dots), Deuterium (open circles) and Hydrogen (crosses) data, (b) to all data sets combined. The solid lines are the best estimates of λ and r_G; the dashed lines show their 1σ variation, taken as a linear sum of statistical and systematical errors.

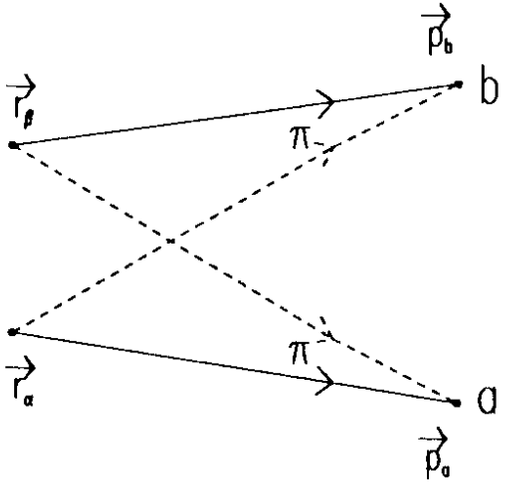
$\vec{p}_b$
b
$\vec{r}_\beta$
π^-
π^+
$\vec{r}_\alpha$
a
$\vec{p}_a$

Fig.1

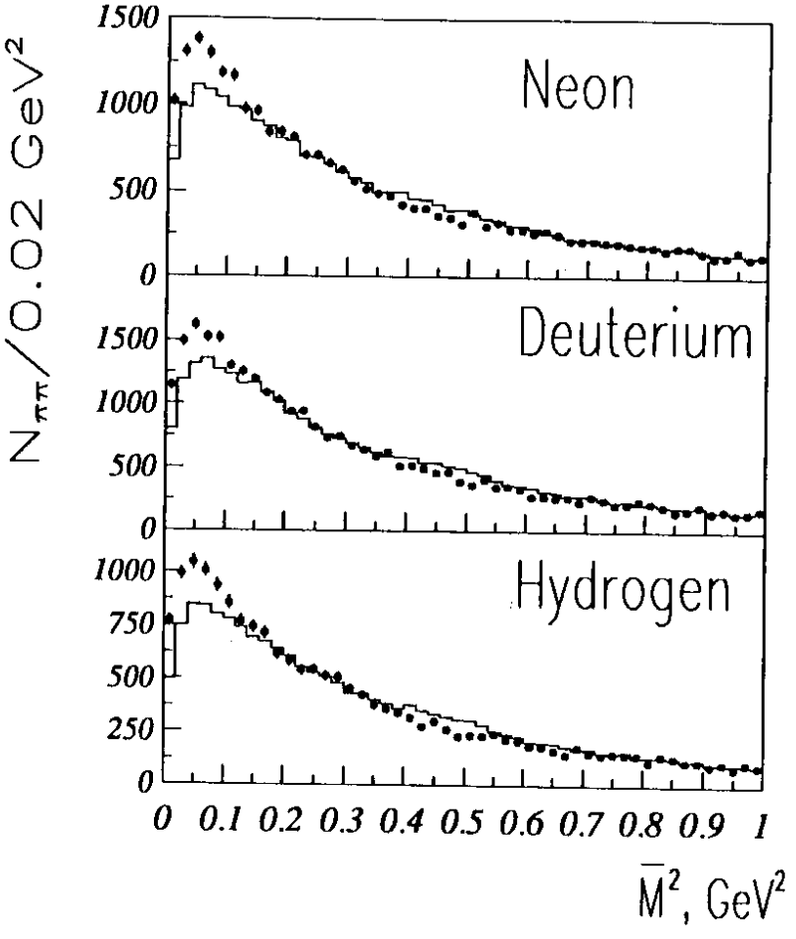
$N_{\pi\pi}$/0.02 GeV^2
Neon
Deuterium
Hydrogen
1500
1000
500
0
1500
1000
500
0
1000
750
500
250
0
0 0.1 0.2 0.3 0.4 0.5 0.6 0.7 0.8 0.9 1
$\bar{M}^2$, GeV^2

Fig.2

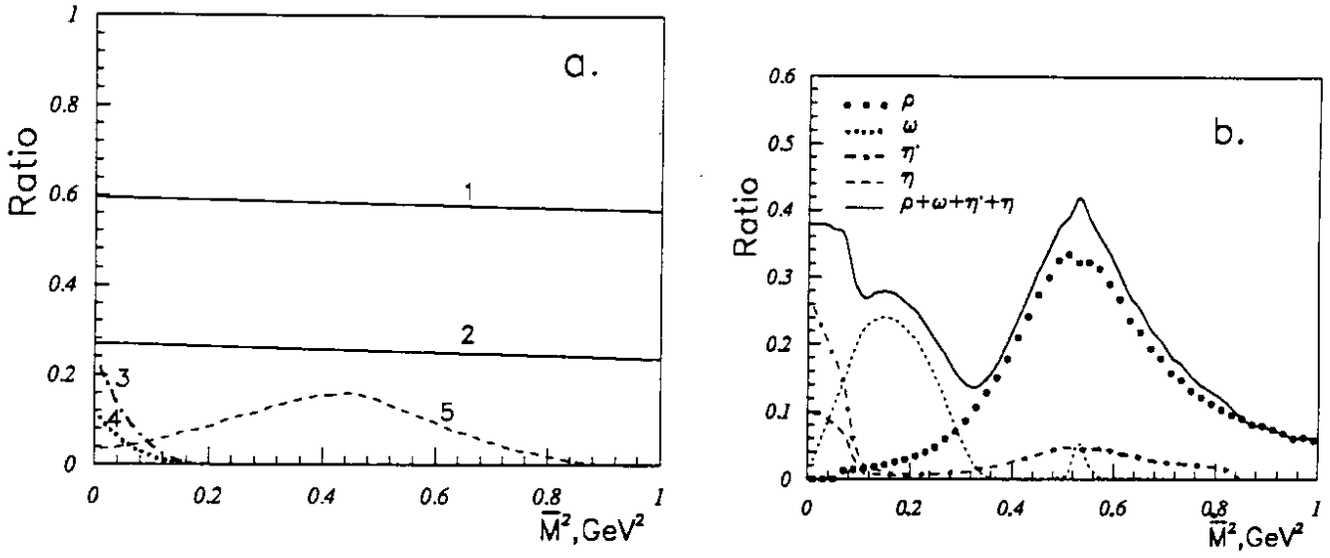

Fig.3

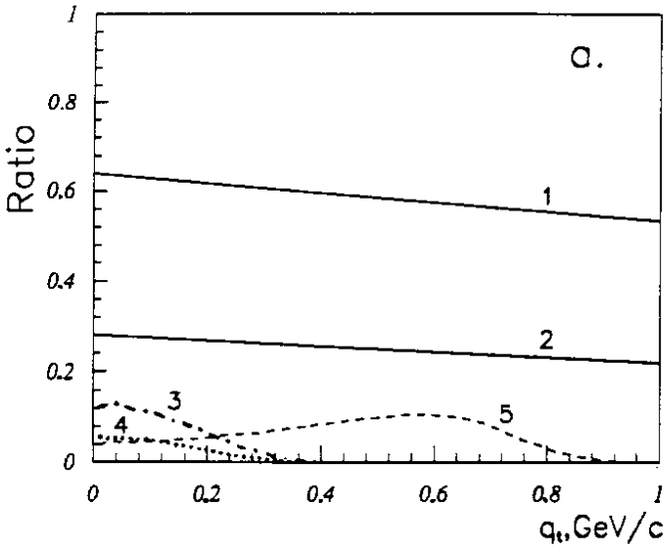
a.
Ratio
1
2
3
4
5
0
0.2
0.4
0.6
0.8
1
q_t,GeV/c

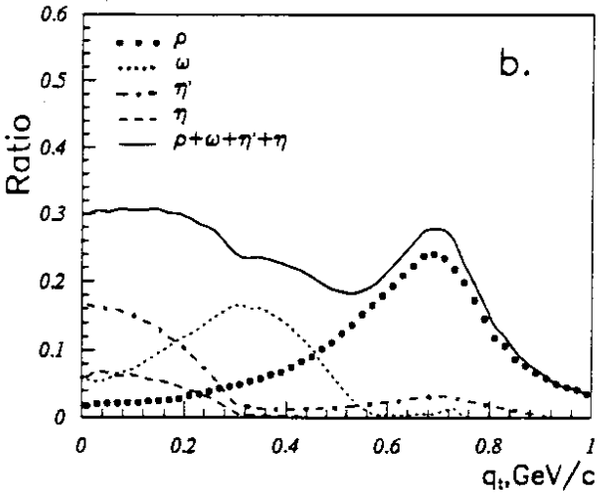
b.
Ratio
ρ
ω
η'
η
ρ+ω+η'+η
0
0.1
0.2
0.3
0.4
0.5
0.6
0.8
1
q_t,GeV/c

Fig.4

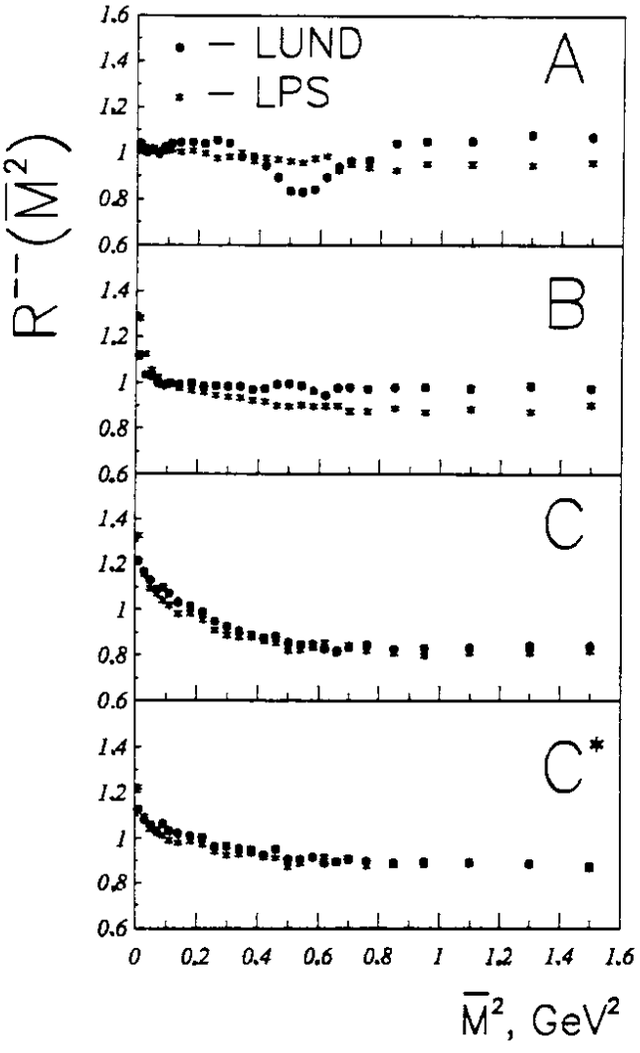
$R^{--}(\bar{M}^2)$
— LUND
— LPS
A
B
C
C*
$\bar{M}^2$, GeV^2

Fig.5a

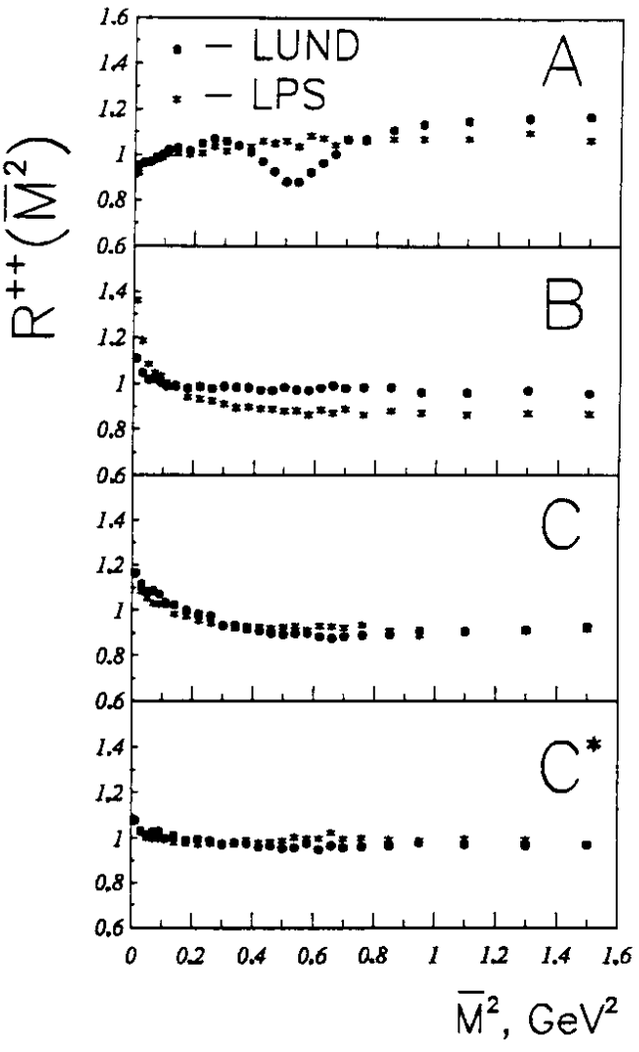
$R^{++}(\bar{M}^2)$
— LUND
— LPS
A
B
C
C*
$\bar{M}^2$, GeV^2

Fig.5b

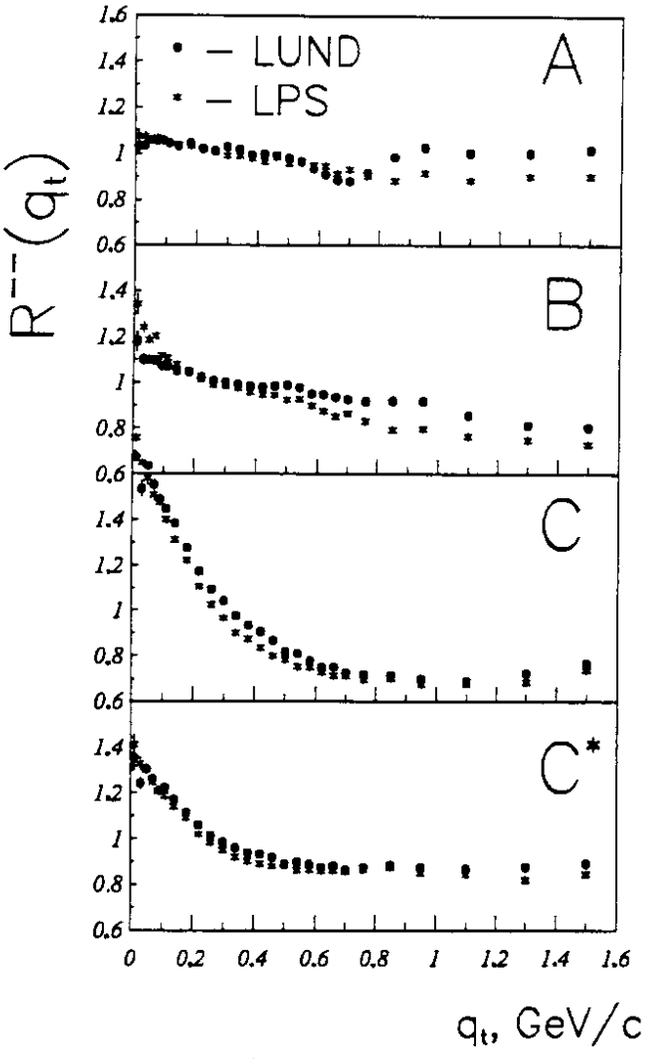

Fig.6a

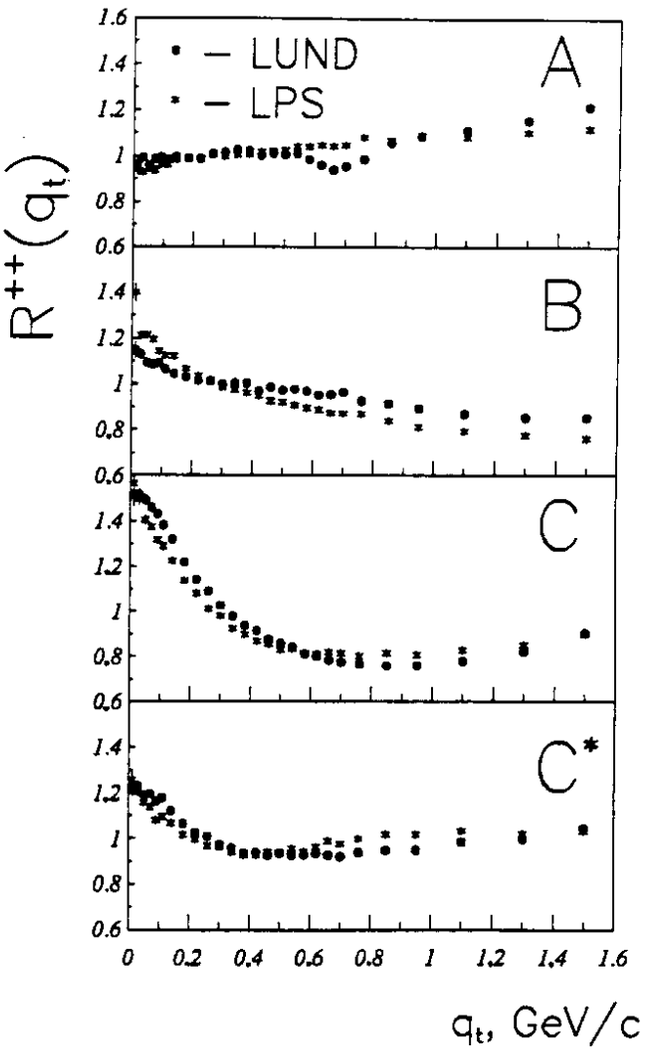

Fig.6b

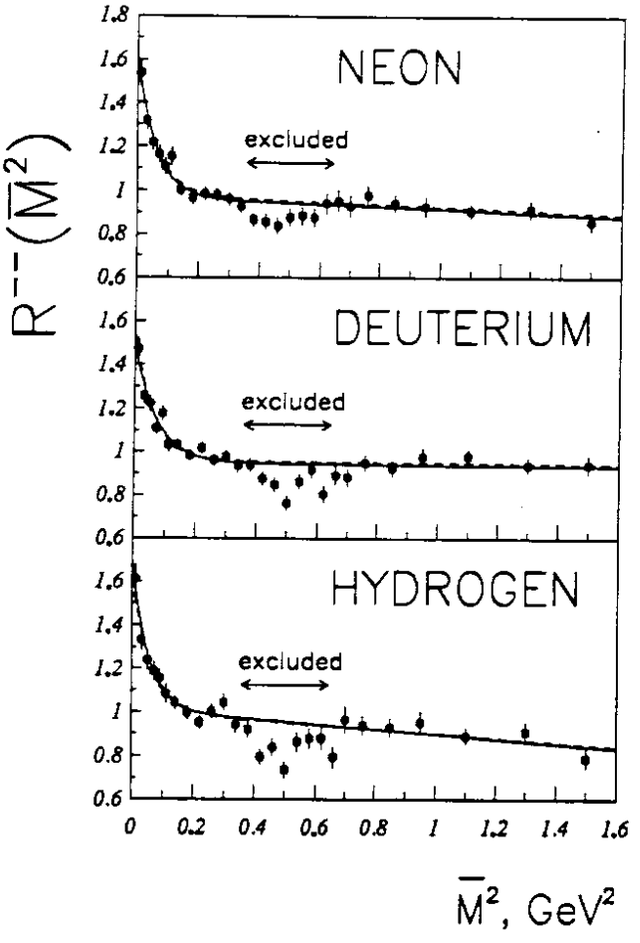
NEON
excluded
DEUTERIUM
excluded
HYDROGEN
excluded
$R^{--}(\bar{M}^2)$
$\bar{M}^2$, GeV^2

Fig.7a

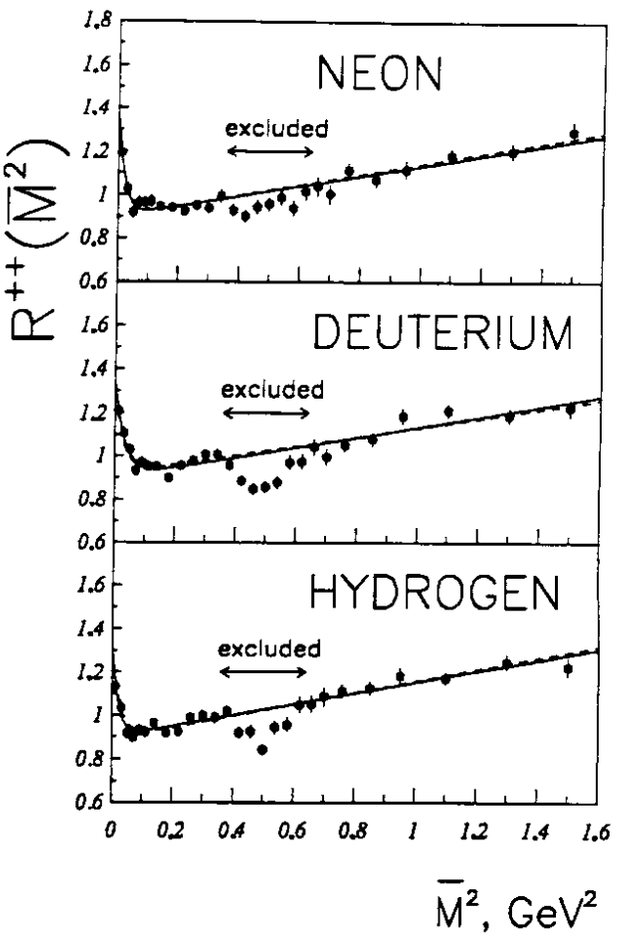
NEON
excluded
DEUTERIUM
excluded
HYDROGEN
excluded
$R^{++}(\bar{M}^2)$
$\bar{M}^2$, GeV^2

Fig.7b

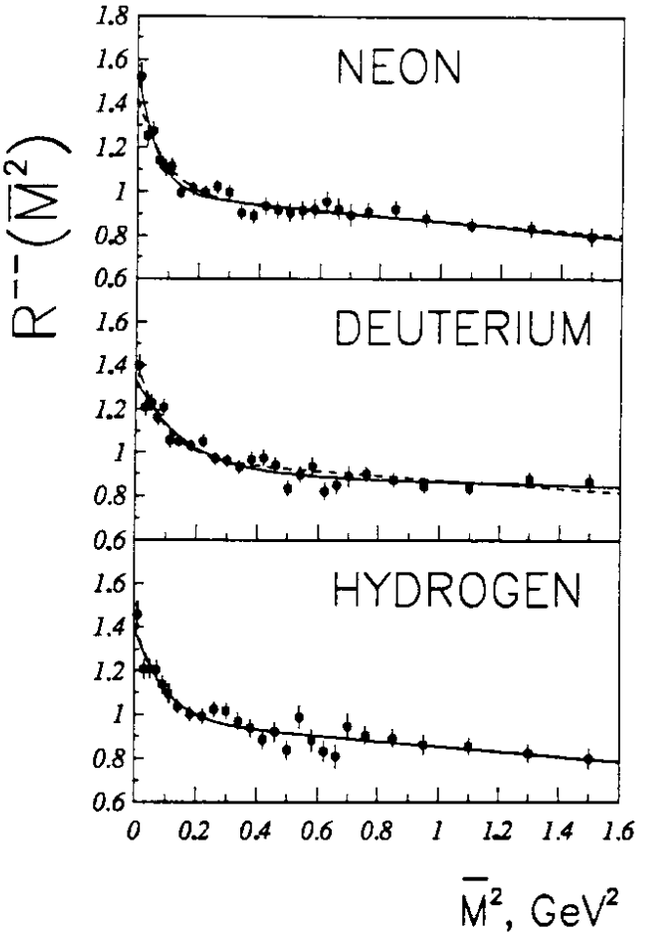
NEON
DEUTERIUM
HYDROGEN
$R^{--}(\bar{M}^2)$
$\bar{M}^2$, GeV^2

Fig.8a

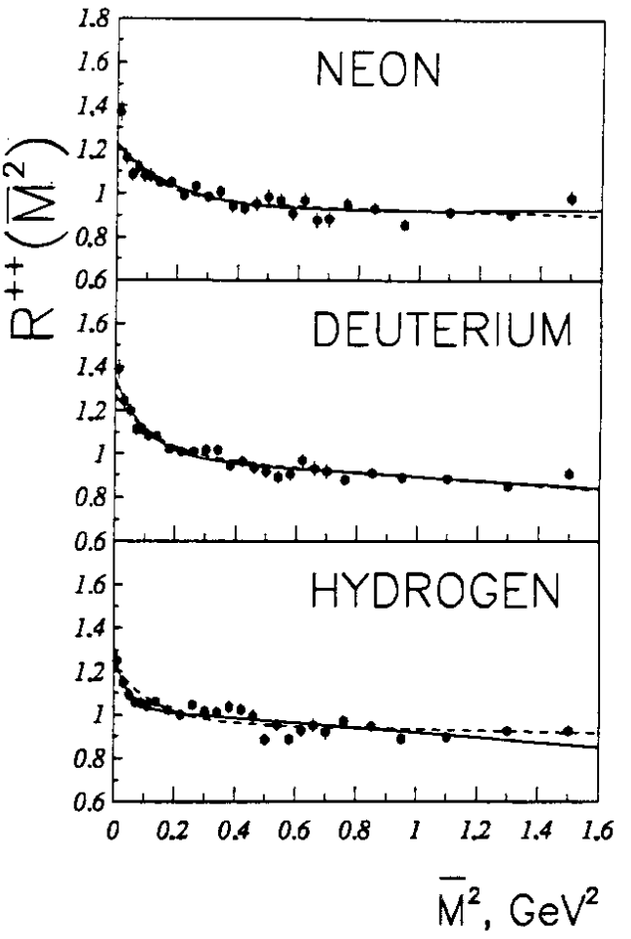
NEON
DEUTERIUM
HYDROGEN
$R^{++}(\bar{M}^2)$
$\bar{M}^2$, GeV^2

Fig.8b

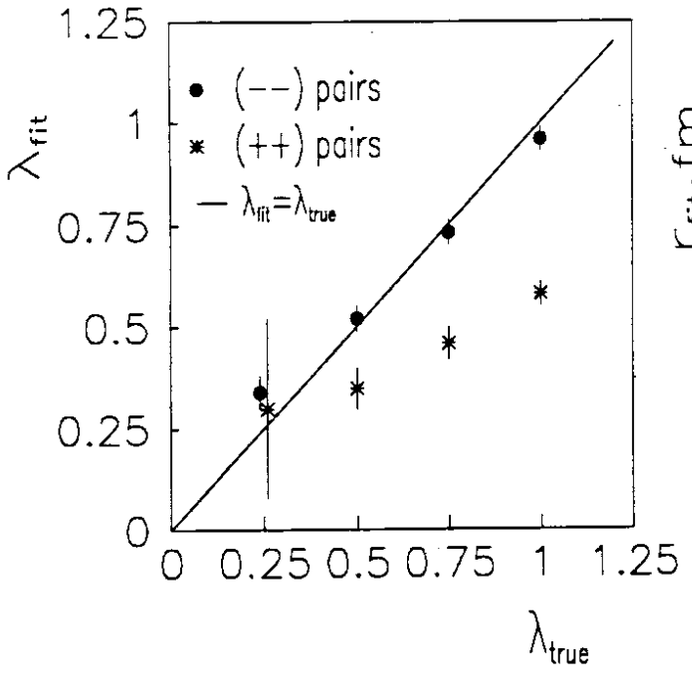
1.25
1
0.75
0.5
0.25
0
0 0.25 0.5 0.75 1 1.25
λ_{fit}
λ_{true}
(--) pairs
(++) pairs
$\lambda_{fit}=\lambda_{true}$

Fig.9a

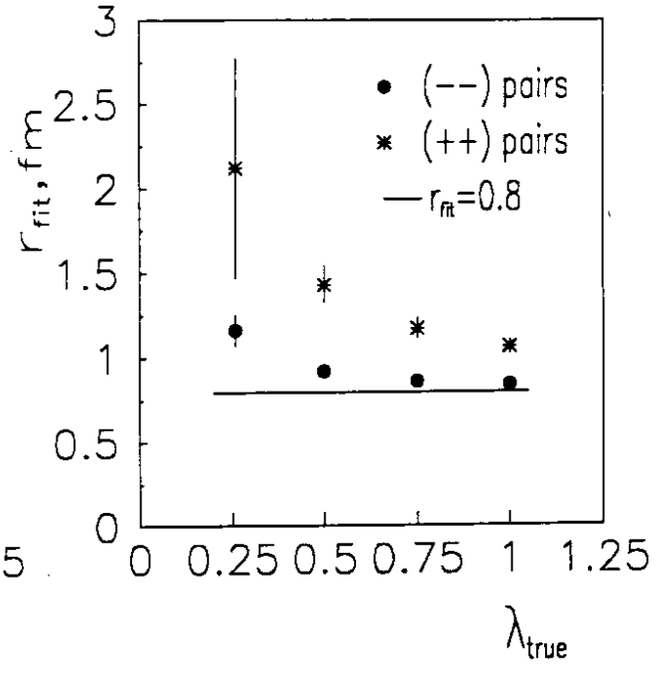
3
2.5
2
1.5
1
0.5
0
0 0.25 0.5 0.75 1 1.25
r_{fit}, fm
λ_{true}
(--) pairs
(++) pairs
$r_{fit}=0.8$

Fig.9b

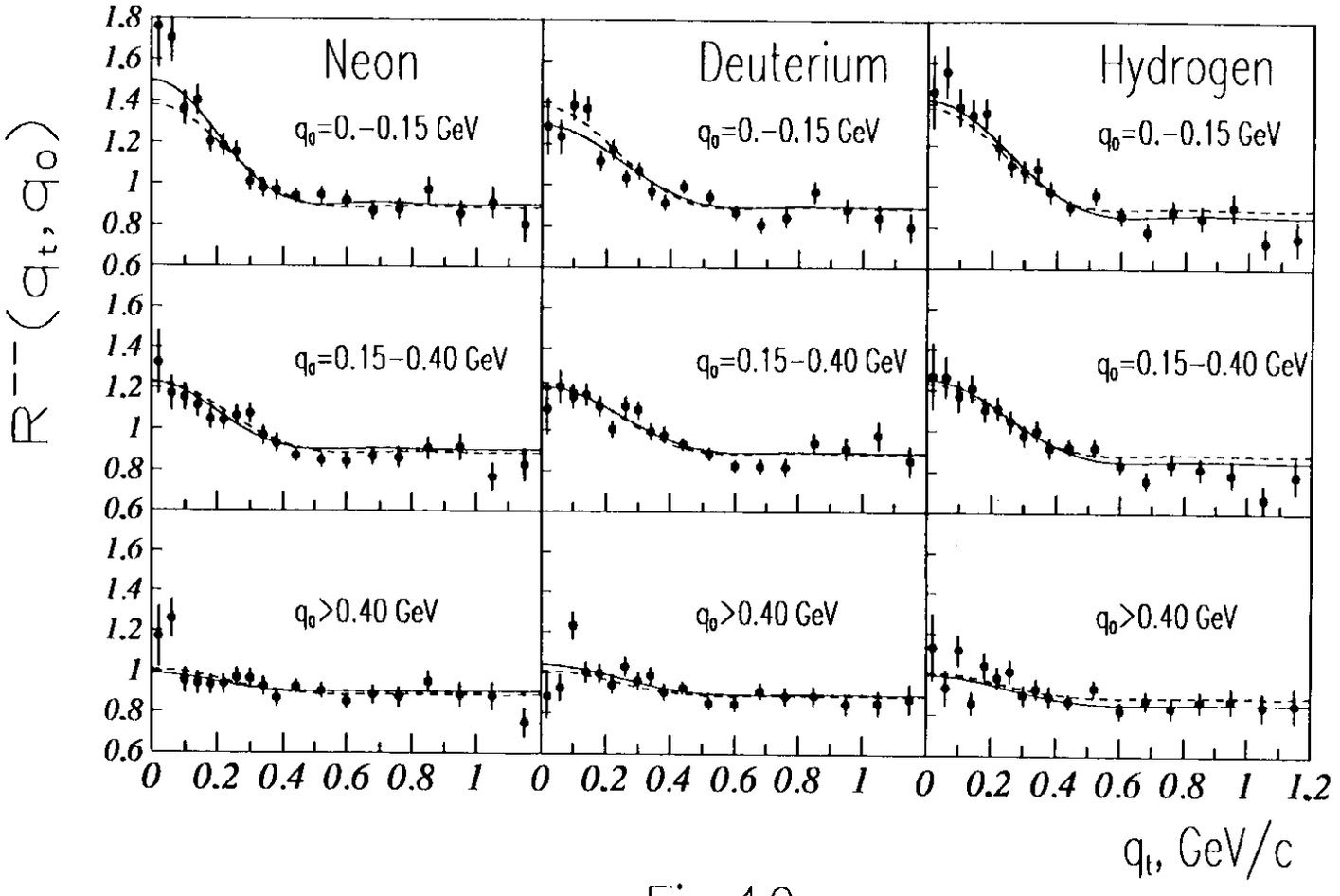
Neon
Deuterium
Hydrogen
q_0=0.–0.15 GeV
q_0=0.15–0.40 GeV
q_0>0.40 GeV
R – 1 (q_t, q_0)
q_t, GeV/c

Fig.10

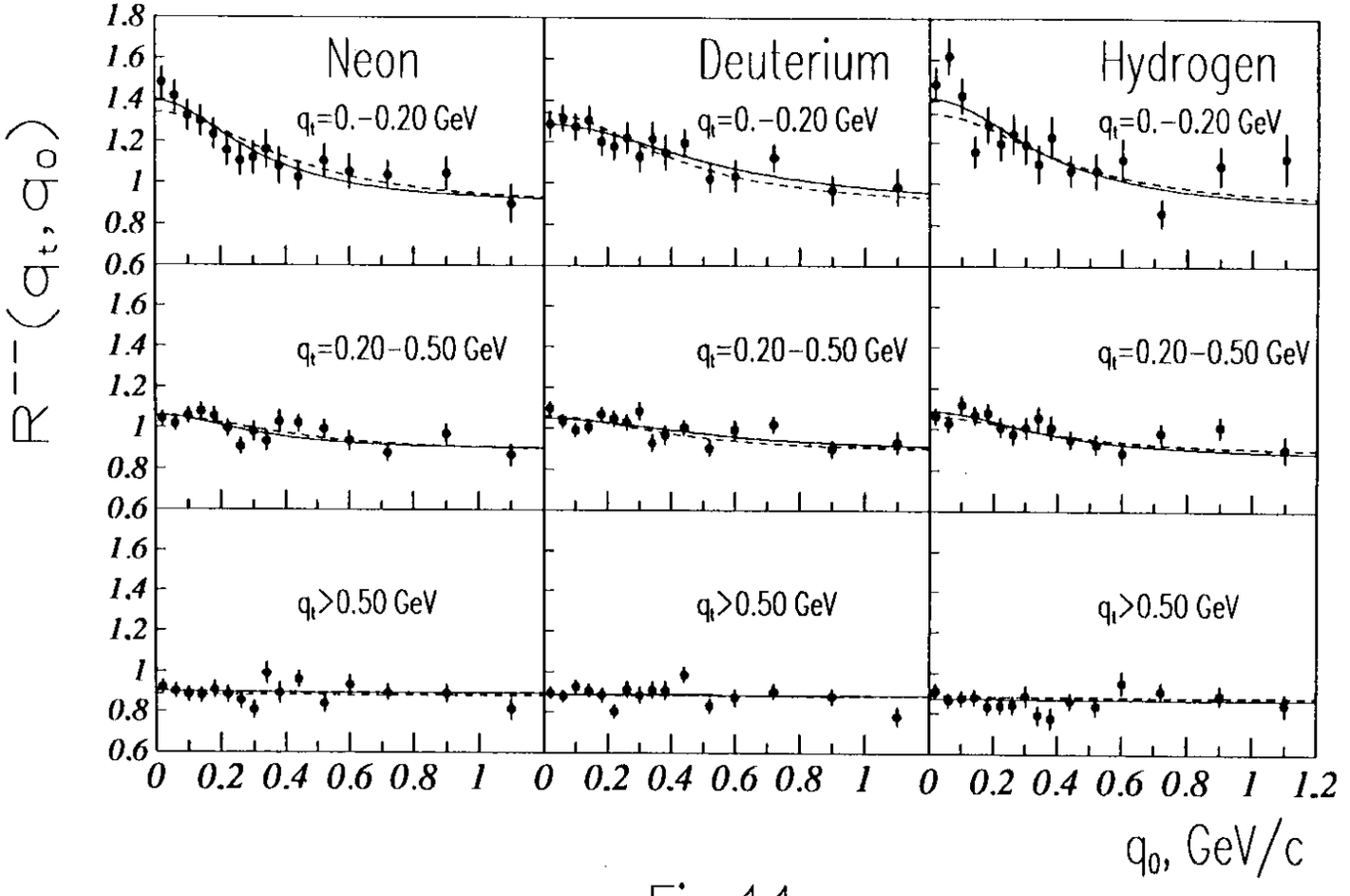
R−(q_t, q_0)
Neon
Deuterium
Hydrogen
q_t=0.−0.20 GeV
q_t=0.20−0.50 GeV
q_t>0.50 GeV
1.8
1.6
1.4
1.2
1
0.8
0.6
0 0.2 0.4 0.6 0.8 1 1.2
q_0, GeV/c

Fig.11

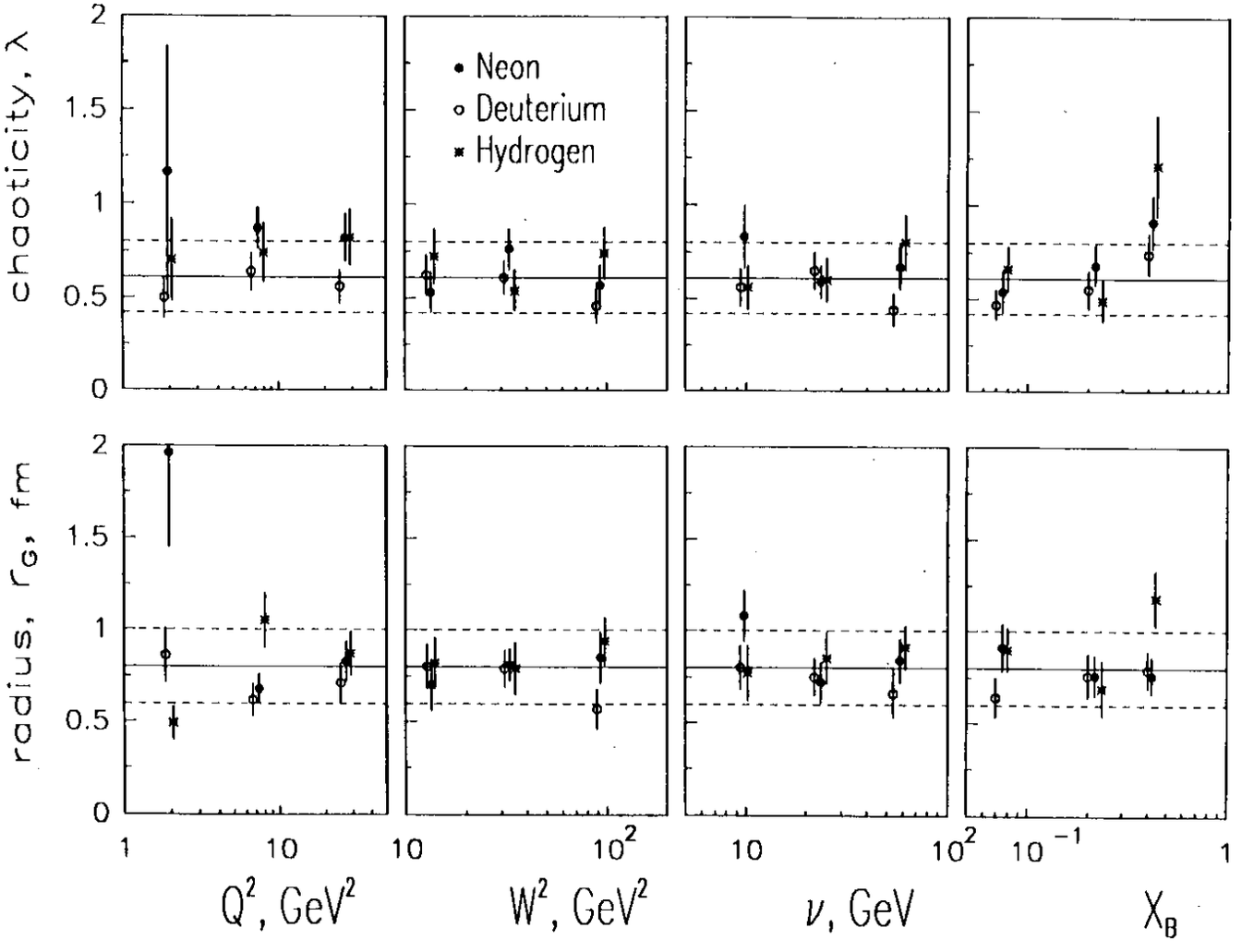
chaoticity, λ
radius, r_0, fm
• Neon
◦ Deuterium
* Hydrogen
Q^2, GeV^2
W^2, GeV^2
ν, GeV
X_B

Fig.12a

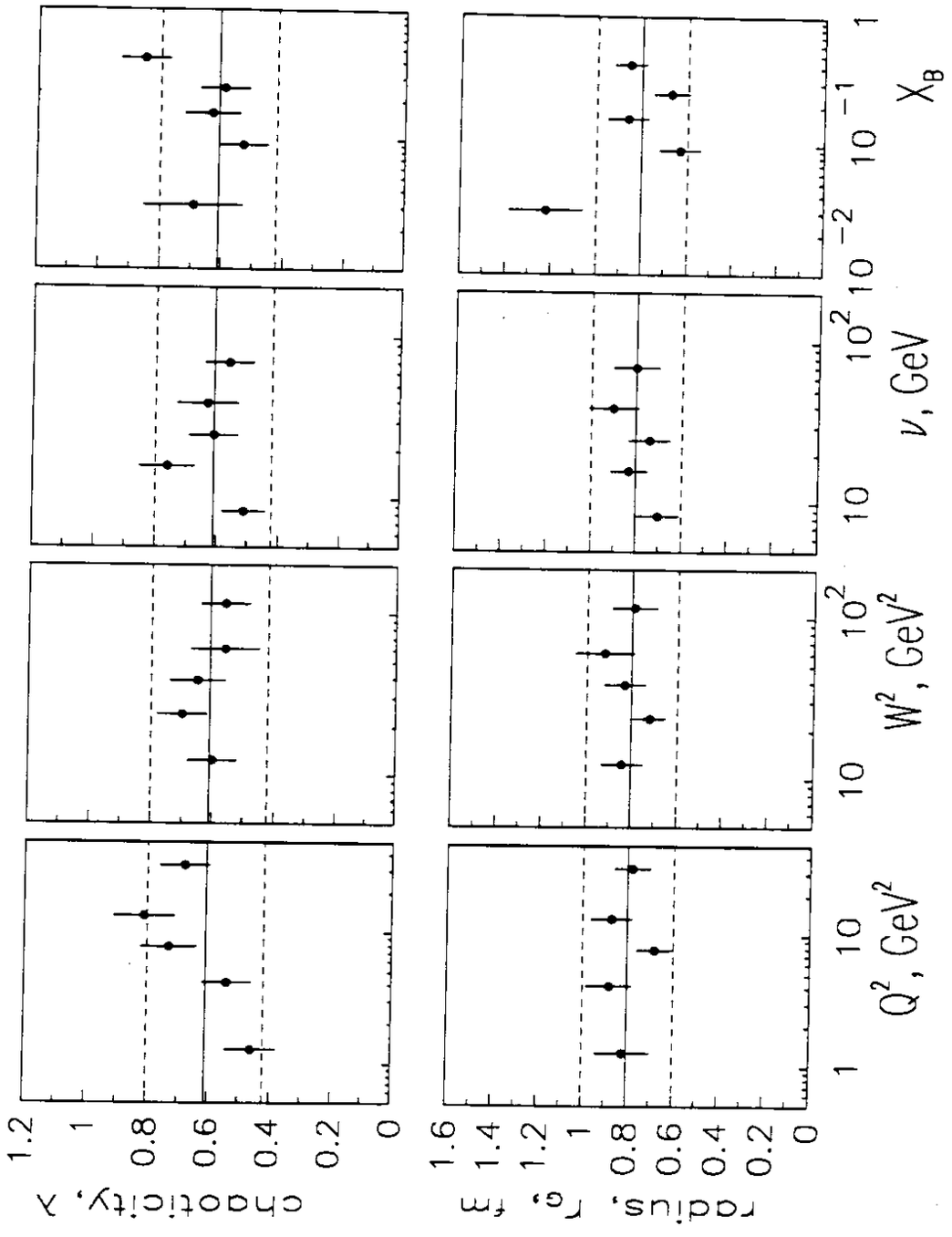

Fig. 12b

Druck: Dokumentationsstelle des Max-Planck-Instituts für extraterrestrische Physik, 8046 Garching